Polym. Korea, Vol. 45, No. 1, pp. 68-78 (2021)
https://doi.org/10.7317/pk.2021.45.1.68

ISSN 0379-153X(Print)
ISSN 2234-8077(Online)

식물성 기름/용매 분리를 위한 Polyaniline-Polyimide 박막 복합 Membrane의 합성과 특성 분석

Naveed Shahzad Ali, Abdul Ghaffar†, Asif Ali Qaiser*, Muhammad Ahmad*, and Khurram

Department of Chemistry, University of Engineering and Technology

*Department of Polymer and Process Engineering, University of Engineering and Technology

(2020년 7월 25일 접수, 2020년 9월 21일 수정, 2020년 9월 23일 채택)

Synthesis and Characterization of Polyaniline-Polyimide Thin-film Composite Membranes for Vegetable Oils/Solvent Separation

Naveed Shahzad Ali, Abdul Ghaffar†, Asif Ali Qaiser*, Muhammad Ahmad*, and Khurram

Department of Chemistry, University of Engineering and Technology, Lahore-54890, Pakistan

**Department of Polymer and Process Engineering, University of Engineering and Technology, Lahore-54890, Pakistan*

(Received July 25, 2020; Revised September 21, 2020; Accepted September 23, 2020)

Abstract: The recovery of solvents from the extracted oils using conventional thermal separation processes i.e. distillation or evaporation is often an energy-intensive process. To provide an energy-efficient alternative, an organic solvent nanofiltration thin-film composite membrane was prepared by depositing a thin layer of polyaniline (PANI), a selective layer, via interfacial polymerization on a crosslinked polyimide (XPI), a base ultrafiltration support membrane, to provide selective transport of constituents of a miscella. The membrane was characterized by microscopic, spectroscopic, and thermal analysis. The evaluation of the separation performance was carried out by a dead-end stirred cell using three vegetable oils. For sunflower, corn, and castor oil/*n*-hexane mixtures, the membrane resulted in a % rejection of 50, 56, and -44, respectively. A comparison of mass flux and rejection of corn and castor oils suggests that the PANI/XPI membranes showed a strong ion-exchange behavior significantly recognizing charge macromolecules due to the presence of charged emeraldine PANI.

Keywords: organic solvent nanofiltration, thin-film composite membrane, interfacial polymerization, crosslinking, vegetable oil/solvent separation.

Introduction

Membrane separation processes are based on the difference in the rate of permeation or diffusion of components in a solution and/or mixture under an applied concentration, pressure, and electric potential gradient. These processes are alternate and replacing more energy-intensive thermal equilibrium processes such as distillation, solvent extraction, and evaporation, etc.[1] Depending on the type of gradient applied, the membrane processes are divided into several categories. These include pressure-driven processes comprising microfiltration (MF), ultrafiltration (UF), nanofiltration (NF), and reverse osmosis (RO); concentration gradient processes comprising membrane dialysis (MD), and pervaporation (PV); electric gradient processes comprising electrodialysis (ED); and temperature gradient process comprising membrane distillation (MD). The diverse division of these processes indicates that the membrane-based separation has become a valuable choice for the separation of constituents of mixture/solution in the industry.[2-5]

The membrane-based separation processes such as MF, UF, NF, RO, ED, and PV are capable to perform separations ranging from 10 μm to < 1 nm. Among these types of separations, nanofiltration can separate constituents ranging from 0.5 to 5 nm and has a strong potential of the separation of organic mixtures/solution that is termed as organic solvent nanofiltration (OSN).[6] Researchers are now focusing on employing polymeric membranes in OSN due to low materials, processing, and operating costs. Solvent resistance is an issue with polymeric OSN membranes that is addressed using various

†To whom correspondence should be addressed.
abdul.ghaffar@uet.edu.pk, ORCID 0000-0002-3794-246X

techniques such as the use of functional fillers, membrane coating, and membrane functionalization, etc. Among those methods, the fabrication of thin-film composite membranes is a promising technique to achieve high flux with commercializable selectivity.[7]

In thin-film composite (TFC) membranes, a thin barrier layer is deposited on a base ultrafiltration support membrane to provide selective transport of constituents of a separating mixture/solution. The top barrier layer may have a different chemical structure than the base UF membrane.[7,8] The most common method of fabricating a thin film on porous support is interfacial solution/vapor phase polymerization whereas other coating techniques are also employed.[9-12]

In TFC membranes, the porous layer can be selected based on various characteristics such as strength, porosity, and resistance to permeating oils and solvents.[8] The mechanical integrity and chemical resistance are obtained by crosslinking the base support layer. Polyimide (PI) has been the focus of many researchers to use as a base polymer with post-casting crosslinking to provide chemical resistance. The crosslinking process is typically carried out using multifunctional amines, alcohols, thiols, or other chemical compounds containing at least one nucleophilic functional group.[13] For composite membranes, polyaniline (PANI) is now considered as a promising polymer capable of generating a functional top layer in TFCs.[14-17] PANI is an intrinsically conducting polymer (ICP) that can be easily synthesized from comparatively low-cost monomers and has many attractive properties such as processability and existence in a variety of oxidation states.[18] The properties of PANI depend mainly on its oxidation/doping states that can be tuned by the ingress/egress of doping anion as shown in Figure 1.[16]

The OSN using a TFC membrane has a strong potential in

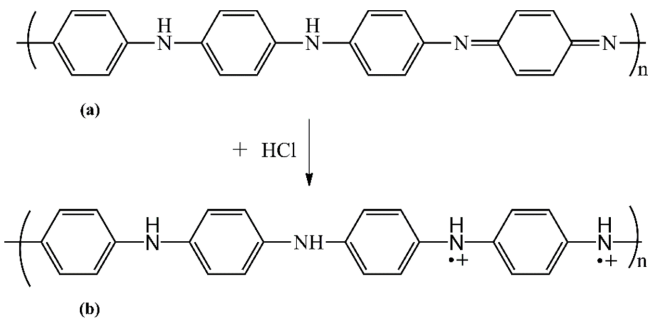

(a) PANI (emeraldine base) (b) PANI (emeraldine salt)

Figure 1. Structural illustration of PANI in emeraldine base and salt states.

the separation of edible oils and fats since the crude form of these oils cannot be utilized commercially without refining and processing to purity. The refining process and extraction of these edible oils from crushed seeds utilizes organic solvents such as *n*-hexane. After oil extraction, these oils/*n*-hexane solutions are fed to distillation units for the removal of solvents.[19,20] The use of membranes for the removal of solvents from mixtures is now being widely studied.[20,21] Pagliero *et al*.[22] studied the degumming of sunflower oil/*n*-hexane micelles using PVDF membranes operating at 4 to 6 bar. Koseoglu *et al*.[23] studied the nanofiltration membranes for the removal of *n*-hexane, ethanol, and IPA from cottonseed oil, and a comparison was shown using polyamide, cellulose acetate, and polysulfone nanofiltration membranes. Wu *et al*.[24] used ceramic membranes for the separation of soybean oil from *n*-hexane and achieved a 20% oil rejection. Rama *et al*.[25] reported the use of *n*-hexane resistant membranes for application in soybean/*n*-hexane degumming achieving an oil rejection of 45% at 2.76 MPa and volumetric flux of 9 L m^{-2} h^{-1}. Kuk *et al*.[26] utilized polyamide membranes for an application in the degumming of cottonseed oil/*n*-hexane miscella with 99% solvent recovery but at lower volumetric fluxes.

The objective of the present work is to fabricate a TFC membrane for OSN of various vegetable oils from *n*-hexane. Electroactive polyaniline was used as a thin barrier layer that was deposited by *in situ* solution phase polymerization on a crosslinked polyimide (XPI) base UF support. The XPI UF membrane was made in-house by crosslinking PI after membrane casting and phase inversion. These PANI/XPI membranes showed improved physical, chemical, thermal, and morphological properties suitable for pressure-driven processes to separate *n*-hexane from vegetable oils (sunflower/corn/castor oil) in the oil extraction plants and refineries. The study comprised TFC membrane fabrication, post-treatment with electroactive PANI followed by structural, thermal, morphological characterization, and testing the membrane performance for OSN use in a dead-end stirred cell.

Experimental

Materials. PI P84® was provided by HP Polymer GmbH (Lenzing, Austria). Ethanol (EtOH), *n*-hexane, isopropanol (IPA), and dimethylformamide (DMF) were purchased from VWR Chemicals (Belgium), Aniline, iron(III) chloride-6-hydrate ($FeCl_3 \cdot 6H_2O$), and hydrochloric acid (HCl) were obtained from Sigma-Aldrich (USA). H_2O_2 (30%) was pur-

chased from Merck (Germany). The nonwoven fiber polypropylene/polyethylene (PP/PE) Novatex 2471 was imported from Freudenberg (Germany). 1,6-hexane diamine (HDA) was purchased from Daejung (Korea). Edible oils comprising sunflower oil, corn oil, and castor oil were purchased from hamza vegetable oil refinery, dalda foods limited, and marhaba laboratories respectively. These edible oils were then utilized to prepare oil/*n*-hexane miscellas. All other chemicals were used as received from the manufacturers. Deionized (DI) water was used throughout the experimental work.

Fabrication of PI UF Support Membranes. PI dope solution was prepared by dissolving PI P84® 24% (w/w) in DMF and stirred for 20 h to form a homogeneous solution. The solution was then allowed to stand for 12 h for degassing as described elsewhere.[27] This viscous solution was then spread on PE/PP Novatex 2471 non-woven fabric with a manual casting blade (Sheen, UK) set at a thickness of 250 μm at room temperature. The cast membrane was then immersed in a DI water bath for the phase inversion.[16] The DI water was replaced thrice with fresh DI water to ensure the complete removal of the solvent. Further, the removal of any residue DMF and water was done by immersing this membrane in an isopropanol bath. The UF support membranes were crosslinked by immersing these membranes in 5% w/v HDA solution in isopropanol for 16 h at room temperature as described by Gorgojo *et al.*[13] The membranes were then washed with IPA for 2 h to completely remove any residual HDA. For further TFC membrane preparation, the membranes were kept in IPA to avoid pore collapse. To ensure repeatability of results, three membrane replicas were prepared. Figure 2 below illustrates the crosslinking scheme for the PI membrane with HDA.

***In-situ* Polymerization of PANI on XPI Membranes.** The XPI support membrane was treated with H_2SO_4/H_2O_2 (3/1 by v/v) for 10 s followed by complete rinsing with DI water. Then *in situ* polymerization of aniline was carried out on the surface of XPI, to prepare the UF membrane according to Chen *et al.*[28] A thin coating of PANI was developed on the XPI surface by soaking PI membrane in 0.09 M aniline solution in 1 M HCl at 0 °C. After the soaking for 24 h, the membranes were immersed in an oxidizing 0.4 M solution of $FeCl_3 \cdot 6H_2O$ in 2 M HCl to initiate the polymerization process. After the formation of a thin coating of PANI on the XPI membrane, the loosely bonded PANI was washed with water followed by washing with 1 M HCl solution. Finally, the developed thin-film composite membranes TFC (PANI/XPI) were washed several times with DI water.

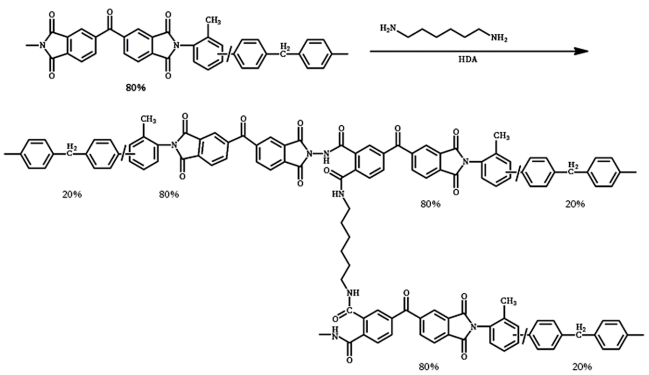

Figure 2. Illustration of the reaction mechanism of crosslinking of PI chain with HDA.

Structural and Thermal Characterization of TFC (PANI/XPI) Membranes. The synthesized TFC (PANI/XPI) membranes were characterized by scanning electron microscopy (SEM), Fourier transform infrared spectroscopy (FTIR), atomic force microscopy (AFM), and thermogravimetric analysis (TGA). The surface and cross-sectional morphology of the membranes were characterized by FEI Nova 450 NanoSEM. Membrane specimens were dried in the vacuum drying oven at 35 °C for 24 h after that sample membranes were mounted on support using conductive paste. The thin layer of gold (Au) (1.5-2.0 nm) was sputtered on each membrane sample using Denton Vacuum Desk V. SEM working conditions were: a 5.6 mm working distance, mode SE, an accelerating voltage 15.0 kV, an emission current 91.9 mA. After coating, the membrane samples were inserted into the field emission SEM and imaged for cross-sectional and surface morphology. To confirm the crosslinking of PI membranes, FTIR in transmittance mode, before and after crosslinking was recorded at 22-24 °C with alpha Bruker, FTIR spectrometer in wavenumber 4000-600 cm^{-1}.[29] AFM topography was carried out to define root mean square roughness (*R*q), average roughness (*R*a), and peak-to-valley height (*R*z) of UF PI, XPI, and PANI coated TFC (PANI/XPI) membranes. Surface topographies of the prepared membranes in the two-dimensional (2D) and three-dimensional (3D) were observed in tapping mode with XE-7 (AFM, Park Systems Suwon, Korea). The root means square (*R*rms) roughness of three regions of membranes were computed by using Origin software. Samples were scanned with TM silicone 10 nm cantilever employing 1.3 Hz scanning frequency. Thermal stability of all the fabricated membranes i.e., unmodified PI, XPI, and TFC (PANI/XPI) membranes were tested using TGA-50 (TGA, Shimadzu, Japan). In each run, about 5-6 mg of each membrane samples were loaded into an

aluminum (Al) pan and heated in a temperature range of 35-600 ºC at the rate of heating, 10 °C/min. The nitrogen flow rate was maintained at 35 mL/min.

Membrane Performance Characterization. The Nanofiltration tests were carried at a pressure of 15-28 bars using locally fabricated benchtop dead-end stirred cell as shown in Figure 3. The effective area of membrane coupons was 0.008533 m^2.

The mass fluxes (J_i) for permeating species was calculated using eq. (1) given below.[30]

$$(J_i) = \frac{m}{A\Delta T} \quad (1)$$

Permeance (L) studies were calculated by dividing the flux with trans-membrane pressure (TMP) as under eq. (2).[31]

$$L = \frac{J_i}{TMP} \quad (2)$$

Experimental rejection (percentage retention R%) of the concentration of oil i was determined by using eq. (3).[14]

$$R\% = \left(1 - \frac{C_{\text{permeate } i}}{C_{\text{feed } i}}\right) \times 100 \quad (3)$$

A mass balance was also calculated to find out material loss in each run of the filtration process. Systematic steps were adopted to minimize the mass loss in each run and keep it in a feasible range of <6-10% by using the eq. (4).[32]

$$\text{Mass balance } i\ (\%) = \frac{V_{\text{permeate}} C_{\text{permeate},i} + V_{\text{retentate}} C_{\text{retentate},i}}{V_{\text{feed}} C_{\text{feed},i}} \times 100 \quad (4)$$

Simulated 100 g sample of two-component i.e. oil/*n*-hexane mixture with w/w% was loaded in the dead-end stirred cell as shown in Figure 3. The oils used were edible triglyceride oils of sunflower, corn, and castor oil. The compositional structure of these oils with physical properties are given in Table 1. PTFE coated magnetic stir bar rotated in the filtration cell above the surface of the TFC (PANI/XPI) membrane under the investigation of separation study to avoid concentration polarization. When approximately 50% volume of the feed solution permeated through the TFC (PANI/XPI) membrane, then the filtration experiment was stopped.[32] The sample collection container was small holed and surrounded by ice to avoid evaporation of the solvents. Solvent flux, permeance, and rejections were calculated with the help of eqs. (1)-(3). The separation test of each solvent mixture was repeated thrice and average values were used for membrane performance calculations.[33]

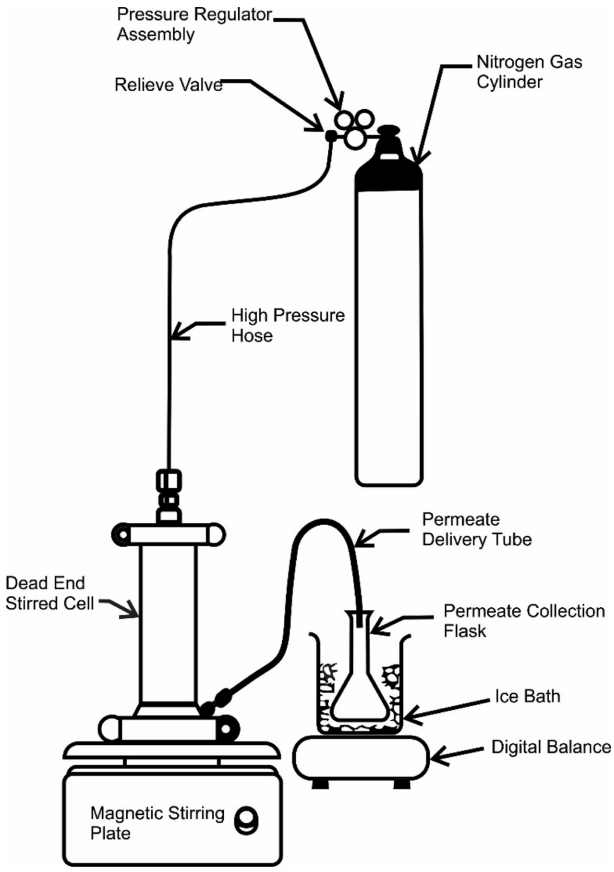

Figure 3. Schematic diagram of the testing apparatus used in the separation studies.

The concentration (mass oil/mass of miscella) of oil in the oil/*n*-hexane sample (permeate) was determined by the solvent evaporation method. In a glass beaker, a known mass of the oil/*n*-hexane sample was added (ms). The sample was then placed into a vacuum oven at 77-120 °C overnight to ensure complete evaporation of *n*-hexane. The beaker containing the residual oil was left to cool down to ambient temperature and then weighed (mr). The mass fraction of the oil i (C_{oil}) in the sample was calculated by using eq. (5).[34]

$$C_{\text{oil}} = \frac{ms - mr}{ms} \quad (5)$$

Results and Discussion

Scanning Electron Microscopic Analysis. SEM micrographs captured at a 10000x magnification of PI, XPI, and TFC (PANI/XPI) membranes are shown in Figure 4. The surface morphology of the uncrosslinked PI membrane showed a defect-free top nanoporous layer at the top of the UF mem-

Table 1. Physical Characteristics of Oils Used in the Separation Studies[55,56]

Sr. No	Oil name	Density (g/cm^3)	Molecular weight (MW) ($g\ mol^{-1}$)	Fatty acids present in the triglyceride oil	Percentage (%)	Name and structures of fatty acids	
						Acid name	Structure
1	Sunflower oil	~0.932	877.92	Palmitic acid	5	Palmitic acid	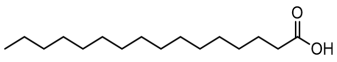
				Stearic acid	6		
				Oleic acid	30	Stearic acid	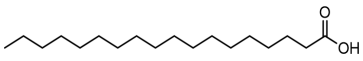
				Linoleic acid	59		
2	Corn oil	~0.916	872.52	Palmitic acid	11	Oleic acid	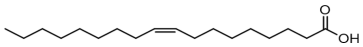
				Stearic acid	2		
				Oleic acid	27		
				Linolenic	1		
				Linoleic acid	58	Linoleic acid	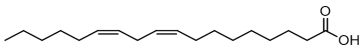
3	Castor oil	~0.961	927.00	Ricinoleic acid	85-95		
				Oleic acid	2-6	Linolenic acid	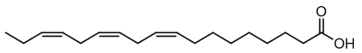
				Linoleic acid	1-5		
				Linolenic acid	0.5–1	Ricinoleic acid	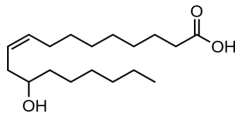
				Stearic acid	0.5-1		
				Palmitic acid	0.5-1		
				Dihydroxy stearic acid	0.3–0.5		
				Others	0.2-0.5	Dihydroxy stearic acid	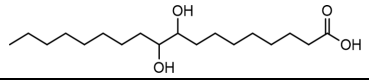

brane base (Figure 4(a)). The cross-section of the PI membrane showed a sponge-like structure with micro-voids (Figure 4(b)). The sponge-like structure was typically generated by solution casting followed by phase inversion[33] because of the exchange of DMF from the membrane into the water bath. The DMF and water have a considerable difference in their solubility parameters that makes the solvent exchange process relatively slower.[35] PI surface micrograph showed a smoother top layer whereas the XPI showed a relatively rougher surface. The cross-sectional images of XPI showed a closed-cell structure as compared to PI (Figure 4(b) *vs*. 4(d)) that was a result of successful crosslinking in membrane bulk. In TFC (PANI/XPI) membranes, the surface morphology showed a broken dense PANI layer at the top of the UF XPI membrane. PANI started growing in nodular shape in nanoscale at the surface that is further extended throughout the surface of the membrane forming a continuous layer.[36,37] The cross-sectional micrograph in Figure 4(f) for TFC (PANI/XPI) membranes depicted a successful fabrication of TFC with a PANI layer (1-2 μm thickness) at the top of UF porous XPI membrane support (Figure 4(f)).

Fourier Transform Infrared Spectroscopy Analysis. FTIR spectra of three membrane samples are shown in Figure 5. In pristine PI membranes the characteristic peaks appeared at 1779 cm^{-1} for carbonyl stretch in imide, peak at 1720 cm^{-1} was assigned to asymmetric stretching of carbonyl in imide, 1364 cm^{-1} was assigned to C-N stretch in imide, 721 cm^{-1} is associated with the C-H vibrations, and 1510 cm^{-1} appeared due to C-C stretch in the aromatic ring.[38]

For XPI membranes, the peak at 1720 cm^{-1} for carbonyl in imide lowered in intensity which depicts the disappearance of imide bands showing the formation of crosslinks with the HDA. This disappearance of carbonyl imide peak is due to the addition of crosslinking moieties as explained elsewhere.[39] The formation of crosslinks resulted due to the cleavage of the C-N bond in the imide of PI main chain. Whereas, the resulting instability of the atomic structure was stabilized by the formation of amide bond which appeared at 1648 and 1539 cm^{-1} due to C-N stretch in combination with N-H bending.[40] Moreover, for the PI IR peaks such as 1779, 1370, 727, and 1539 cm^{-1}, a minor shift was observed along with a decrease in the intensity.

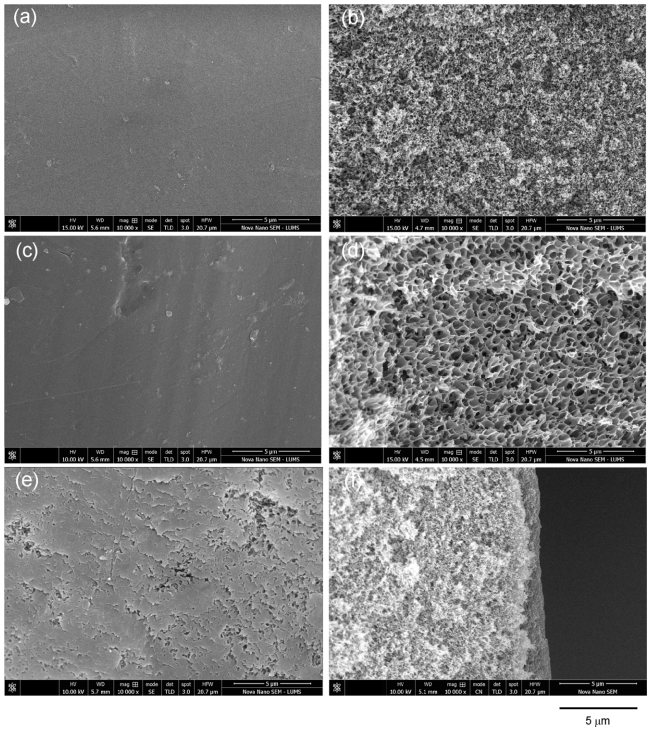

Figure 4. SEM micrographs of membranes at 10000x. Surface and cross-section images of (a) & (b) pristine PI support membrane; (c) & (d) crosslinked PI; (e) & (f) TFC (PANI/XPI) membrane, respectively.

For PANI deposited XPI membranes (PANI/XPI), the increase in the intensity of the IR curve depicts the layering of the membrane and a shift was observed for the PANI characteristic peaks. The characteristic quinoid peak appeared at 1647 cm^{-1}, the benzenoid peak appeared at 1540 cm^{-1}, aromatic C-H vibrational peak appeared at 823 cm^{-1}, and =N- in quinoid appeared at 1089 cm^{-1}. However, the peak for C-N vibration remained unchanged at 1306 cm^{-1}. The shift in the peak for N- in quinoid may be attributed to weak attractive forces in the unreacted HDA. The presence of both PI and PANI peaks in the PANI/XPI membranes depicts that the XPI membranes are finely coated with the PANI. Whereas, no prominent decrease in the wavenumber was observed showing that there were least detectable interactive forces in these two polymers. Whereas, the homogeneous coating of the PANI may be due to the similar chain structure of both PANI and PI that assisted in the coating of the membrane.

Atomic Force Microscopic Analysis. In the AFM study, the surface of the membrane was scanned in noncontact mode with a scanning area of 1×1 μm^2. AFM micrographs of the membrane surfaces were shown in 2D-Figure 6 (a, d, and g).

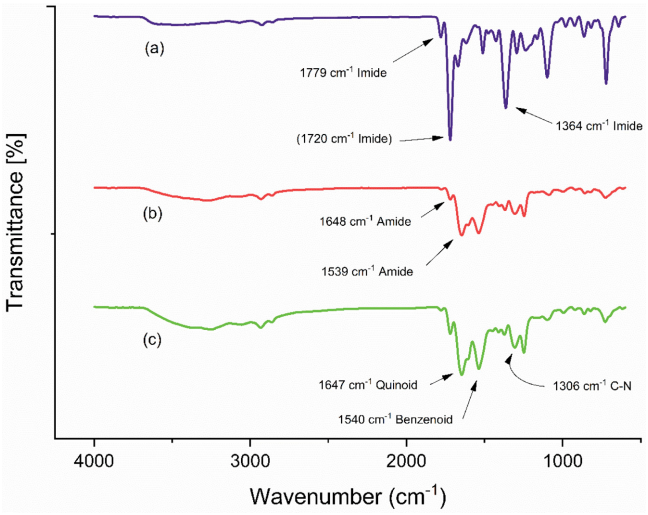

Figure 5. FTIR spectra of (a) PI; (b) XPI; (c) TFC (PANI/XPI) membranes.

These Figures show the surface, surface relief profiles, and extent of the PANI layer on XPI (TFC membranes). 3D images (Figure 6 b, e, and h) also portrays the geometry of pores and surface roughness in vertical directions.[41,42] It was evident from AFM micrographs that PANI deposition was disjointed layer at the surface of XPI, which was also confirmed by Figures 4(f) and 5(c). From AFM images, surface topography, and root-mean-square roughness (R_{rms}) were calculated using the eq. (6).[43]

$$R_{rms} = \frac{\sqrt{\sum_{n-1}^{N}(Zn - Z_{avg})^2}}{N-1} \quad (6)$$

Where Z is height and Z_{avg} is an average value for N number of Zn points in the area (1 μm^2).

It is quite evident from the AFM micrographs and also from the surface relief profiles, that PANI has successfully deposited as a discontinuous thin layer at the surface of XPI during the process of *in situ* polymerization. This small deposition of PANI has increased the selectivity of TFC membranes.[41,44] AFM surface analysis indicates that *R*q, *R*a, and *R*z values increase in the order of PANI/XPI>XPI>PI as shown in Table 2. It was also confirmed by Figure 6 (c, f and i) that surface roughness increases in the same order. These observations yield a close understanding of the molecular designs, resulting from membrane fabrication stages including phase inversion process, *in situ* polymerization, and their impact on the flux, permeance, and %rejection.

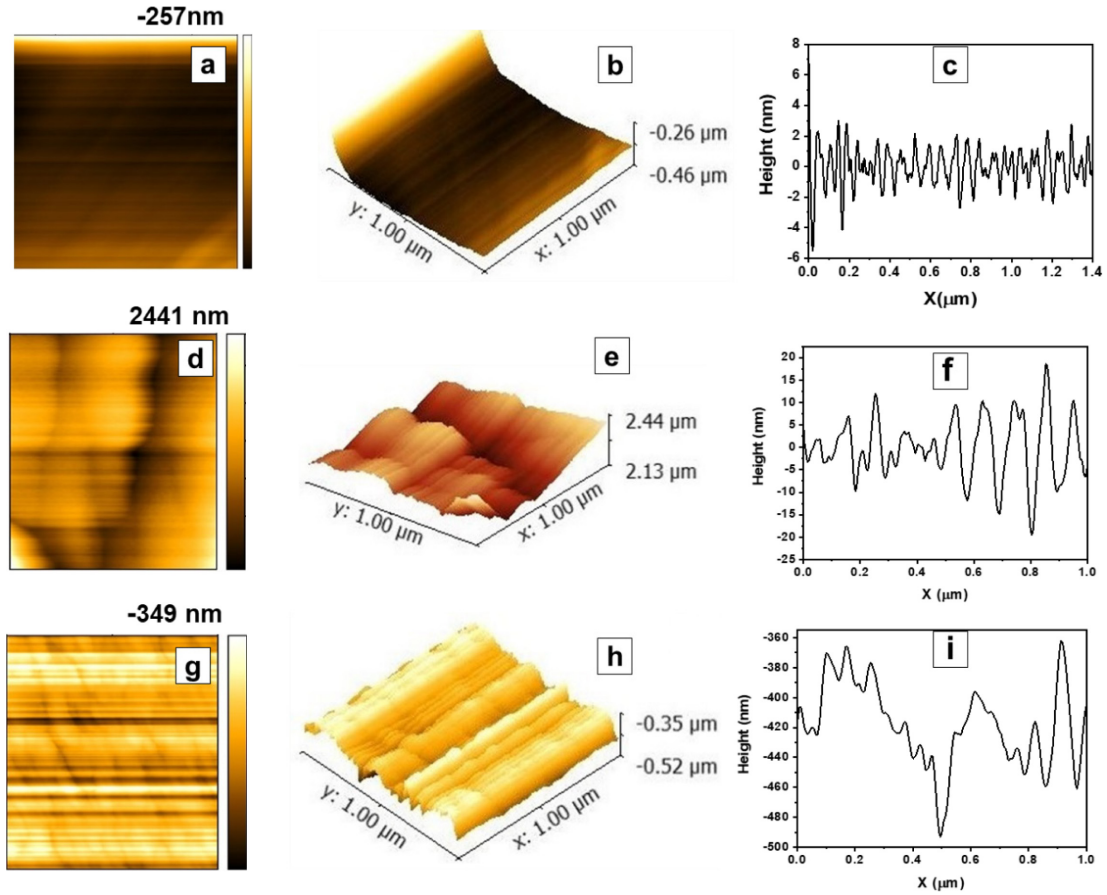

Figure 6. Topographical images 2D, 3D and typical cross-sections profiles of PI uncrosslinked (a-c); XPI (d-f); TFC (PANI/XPI) (g-i) coated films.

Table 2. A Quantitative Data of Surface Roughness of Membrane Samples

No	Membrane description	*R*q (nm)	*R*a (nm)	*R*z (nm)
1	PI	1.3	1.0	7.4
2	XPI	5.9	4.4	24.9
3	TFC (PANI/XPI)	12.7	9.2	54.9

Thermogravimetric Analysis. TGA analysis is used to find the thermal stability and weight loss of the membrane samples as a result of heat treatment. The thermograms of the various fabricated membranes are shown in Figure 7. The pristine PI membrane showed a two-stage thermal degradation. Initially, the insignificant weight loss up to around 100 °C can be attributed to the removal of the residual amount of water and solvents. The PI membrane remained stable up to ~400 °C. Then, at around ~440 °C the second degradation step was observed which lasted up to 600 °C.

This decrease is attributed to the degradation of the main chain of the polymer with subsequent emission of gaseous content and char formation. The resistance to degradation at a temperature <400 °C indicates the high thermal stability of PI.[45] The presence of phenyl groups on the main chain of the PI restricts the movement of main chains. These chains have lower inter chain free volumes. With the addition of cross-linking agents, the free volume of the chains increases.[46] The increase in the free volume results in a decrease in the rigidity of the main chain of the PI and prevents the closer packing of chains. Therefore, a decrease in the thermal stability of the XPI membranes was observed. Here, a four-step degradation was observed. Firstly, up to ~100 °C, the degradation step is associated with the loss of residual solvents which is preferably IPA. The second degradation step initiates at *t* ~200 °C that is associated with the evaporation of unreacted HDA in the membrane structure. At >200 °C, the third degradation step initiates that showed a significant weight loss up to ~430 °C. This decrease in the weight is attributed to the loss of chemically bonded HDA with the PI main chains. The loss of bonded

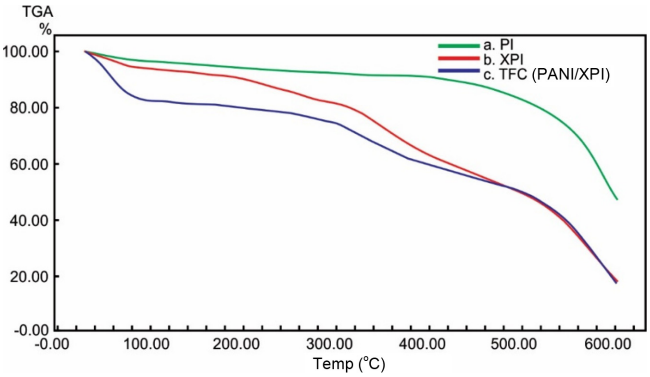

Figure 7. Thermogravimetric analysis of membranes (a) PI (uncrosslinked); (b) XPI; (c) TFC (PANI/XPI).

HDA resulted in a higher temperature than its boiling point due to the energy consumed for the cleavage of the covalent bond.[46] The fourth degradation curve initiates at around ~430 °C and continues up to 600 °C resulting in degradation of the polymer main chain and subsequent release of gaseous content. These degradation curves suggest that the addition of HDA in the PI main chain as a crosslinking agent reduced the thermal stability of the membranes.

For the thin-film composite membrane (PANI/PI), a mixed behavior for thermal degradation was observed. In TFC membranes, a four-step thermal degradation pattern was suggested. Initially, up to ~100 °C, the weight loss is mainly due to the loss of water residing in the membrane structure which was used to make molar acidic solutions to carry out PANI polymerization. Then, the second degradation initiates at ~100 °C and continues up to ~260 °C. This weight loss is attributed to the loss of the dopant anions. Whereas, the third degradation step initiating at ~330 °C up to ~480 °C is attributed to the degradation of the PANI main chains.[47] Whereas, the fourth degradation step is related to the degradation of the PI main chain. The degradation point of the PI main chain is nearly similar in all membranes.

Separation Performance of TFC (PANI/XPI) Membranes. Separation study of oil/*n*-hexane mixtures with TFC (PANI/XPI) membranes was carried out using a dead-end stirred cell. The %rejection and flux of various oil/*n*-hexane mixtures are shown in Table 3. The oils have a molecular weight (MW) order castor oil > sunflower oil > corn oil whereas the %rejection (*R*%) values have an order corn oil > sunflower oil > castor oil that indicates that MW of oils was not the sole factor for separation in the membranes. Sunflower oil, corn oil, and castor oil in *n*-hexane miscella systems showed a rejection of 50, 56, and -44%, respectively. For the sunflower/*n*-hexane system, the oil rejection (*R*%) value is comparable to that given in the literature.[22] Increasing transmembrane pressure increased the rejection of corn oil in the corn oil/*n*-hexane miscella system. This increase in *R*% is accompanied by a higher mass flux of lower molecular weight *n*-hexane as compared to the sunflower/*n*-hexane system that resulted in an increase in the concentration of oil in the retentate. This effect of pressure on the *R*% of oils is also described elsewhere.[48] The *R*% for castor oil suggested that the extraction of oil from the oil/*n*-hexane miscella besides the pressure is also highly dependent upon the polarity of oil in a partially hydrophilic charged nanofiltration PANI/XPI membranes.[48] The negative rejection values are described in the literature in terms of the excessive plasticization of the membrane thus releasing a higher concentration of oil in the permeate.[48] The *R*%, mass flux and permeate values given in Table 3 suggest that the highly polar chain structure of the ricinoleic acid in castor oil due to the presence of hydroxyl group probably interacts with the NH^+ moieties of PANI (ES) chain as shown in Figure 8.[49] The hydrophilic nature of PANI in the emeraldine salt state might have attracted the polar segments of ricinoleic acid in castor oil tri-

Table 3. Separation Performance of TFC (PANI/XPI) Membranes

System	Pressure (bar)	Feed			Permeate			Flux ($g\ m^{-2}\ h^{-1}$)		Permeance ($g\ m^{-2}\ h^{-1}\ Bar^{-1}$)		$R\%=\left(1-\frac{C_p}{C_f}\right)\times 100$
		Oil: *n*-hexane (w/w%)	Volume (cm^3)	Oil Concentration (g/cm^3)	Oil: *n*-hexane (w/w%)	Volume (cm^3)	Oil Concentration (g/cm^3)	Oil	*n*-hexane	*n*-hexane	Oil	
Sunflower/ *n*-hexane	15	25 : 75	138	0.1809	13.01 : 86.98	71	0.0898	372.54	2489.61	165.97	24.83	50
Corn oil/ *n*-hexane	25	25 : 75	139	0.1798	11.6 : 88.3	87	0.0798	410.17	3105.59	124.22	16.40	56
Castor oil/ *n*-hexane	28	10 : 90	145	0.0685	14.13 : 85.86	72	0.0986	388.47	2360.11	84.28	13.87	-44

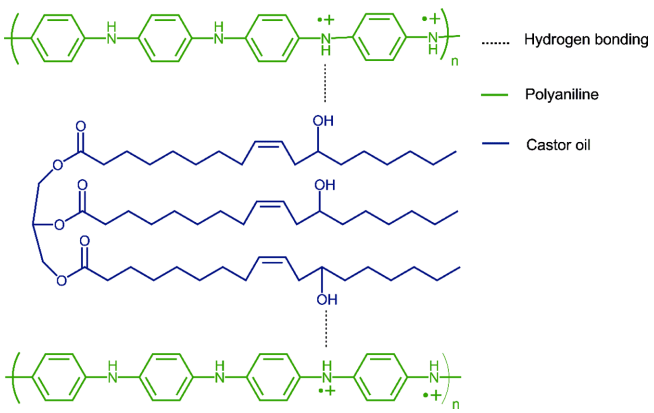

Figure 8. Proposed interaction of PANI and castor oil.

glyceride that resulted in the absorption and retention of the oil in the membrane bulk. The lower mass flux of castor oil with a negative rejection indicates the absorption of castor oil in the membrane bulk with the subsequent release in the permeate under high-pressure gradient across the membrane. The similar behavior of low flux with negative rejection is also described elsewhere for ionic species.[50,51] Moreover, the mass flux of non-polar *n*-hexane decreased significantly as compared to castor oil also suggests the possible selective behavior of the charged moieties developed in the bulk of membrane due to the interaction of OH^- of polar castor oil and NH^+ in PANI (ES) molecular chains. The previous studies have shown that for the separation of high molecular weight solutes from low molecular solvents, the concentration of feed miscella, operating conditions, and structure of the membrane play a controlling role.[51,52] A comparison of mass flux and rejection of corn and castor oils suggests that the PANI/XPI membranes in the present study showed a strong ion-exchange behavior significantly recognizing charge macromolecules due to the presence of charged emeraldine PANI.[53,54]

Conclusions

In this work, we have successfully fabricated TFC membranes by coating a thin layer of PANI, the selective layer, via interfacial polymerization at 0 °C on the XPI surface, a base ultrafiltration support membrane, for the separation of solvent from oil/*n*-hexane mixture. The FTIR analysis confirms the adhesion of PANI on XPI. The SEM micrographs demonstrated a successful fabrication of PANI/XPI TFC membranes. The potential use of PANI for separation of miscella (oil/*n*-hexane mixture) is practically demonstrated by dead-end stirred cell using three vegetable oils. The membrane exhibited a %rejection of 50, 56, and -44 for sunflower, corn, castor oil/*n*-hexane mixtures, respectively. The results also showed that synthesized membranes are chemically stable and having suitable pore size for the separation of *n*-hexane from selected edible/non-edible oils. In addition to that, it was also revealed that charged PANI in the pressure-driven process also interacts with ricinoleic acid, the main constituent of castor oil, resulting in negative rejection. Synthesized TFC membranes may also serve as an alternative energy-efficient separation technique or in combination with conventional thermal separation processes for the separation of vegetable oil and recovery of solvent from the extracted vegetable in the seed-oil industry.

Acknowledgment(s): The authors thankfully recognize the services of COMSATS University Islamabad (Lahore Campus), for providing AFM testing. The authors also pleasantly acknowledge Lahore university of management sciences (LUMS) for the SEM testing service.

References

1. Khulbe, K.; Feng, C.; Matsuura, T. *Synthetic Polymeric Membranes*: *Characterization by Atomic Force Microscopy*; Springer-Verlag Berlin and Heidelberg GmbH & Co. KG: Berlin, Germany, 2008.
2. Nene, S.; Patil, G.; Raghavarao, K. *Membrane Distillation in Food Processing*. In *Handbook of Membrane Separations*; CRC Press: Boca Raton, USA, 2008; 513-551.
3. Schuur, B.; Brouwer, T.; Smink, D.; Sprakel, L. M. J. Green Solvents for Sustainable Separation Processes. *Curr. Opin. Green Sustain. Chem*. **2019**, 18, 57-65.
4. Kiss, A. A.; Lange, J.-P.; Schuur, B.; Brilman, D. W. F.; van der Ham, A. G. J.; Kersten, S. R. A. Separation Technology-making a Difference in Biorefineries. *Biomass Bioenergy* **2016**, 95, 296-309.
5. Sholl, D. S.; Lively, R. P. Seven Chemical Separations to Change the World. *Nature* **2016**, 532, 435-437.
6. Drioli E.; Giorno, L. *Comprehensive Membrane Science and Engineering*; Elsevier: Kidlington, UK, 2010.
7. Vandezande, P.; Gevers, L. E. M.; Vankelecom, I. F. J. Solvent Resistant Nanofiltration: Separating on a Molecular Level. *Chem. Soc. Rev.* **2008**, 37, 365-405.
8. Marchetti, P.; Jimenez Solomon, M. F.; Szekely, G.; Livingston, A. G. Molecular Separation with Organic Solvent Nanofiltration: A Critical Review. *Chem. Rev.* **2014**, 114, 10735-10806.
9. Abegunde, O. O.; Akinlabi, E. T.; Oladijo, O. P.; Akinlabi, S.; Ude, A. U. Overview of Thin Film Deposition Techniques. *AIMS Mater. Sci*. **2019**, 6, 174-199.
10. Qaiser, A. A.; Hyland, M. M.; Patterson, D. A. Polyaniline

Deposition Site Control on Microporous Mixed Cellulose Ester Membranes: Surface and In-pore Polymerization. *IOP Conf. Ser.: Mater. Sci. Eng*. **2009**, 4, 012009.
11. Adamczak, M.; Kamińska, G.; Bohdziewicz, J. Preparation of Polymer Membranes by *In Situ*. *Int. J. Polym. Sci*. **2019**, 6217924.
12. Kim, C.; Jung, A.; Ha, N.; Yeom, B. Conductive Thin Films Composed of Silver Nanowires and Poly(acrylic acid) Prepared by Layer-by-Layer Assembly. *Polym. Korea* **2017**, 41, 681-685.
13. Gorgojo, P.; Jimenez-Solomon, M. F.; Livingston, A. G. Polyamide Thin Film Composite Membranes on Cross-linked Polyimide Supports: Improvement of RO Performance via Activating Solvent. *Desalination* **2014**, 344, 181-188.
14. Chae, D. W.; Choi, H. K.; Jeon, J. Y. Permeation Properties of Copolyimide UF Membrane with Good Thermal Stability. *Polym. Korea* **2016**, 40, 154.
15. Loh, X. X.; Sairam, M.; Bismarck, A.; Steinke, J. H. G.; Livingston, A. G.; Li, K. Crosslinked Integrally Skinned Asymmetric Polyaniline Membranes For Use in Organic Solvents. *J. Membr. Sci*. **2009**, 326, 635-642.
16. Kim, E.; Lee, J. Morphological Changes in the Growth Process of Polyaniline During Galvanostatic Depositon. *Polym. Korea* **2018**, 42, 834-840.
17. Monjezi, S.; Soltanieh, M.; Sanford, A. C.; Park, J. Polyaniline Membranes for Nanofiltration of Solvent from Dewaxed Lube Oil. *Sep. Sci. Technol*. **2018**, 54, 795-802.
18. De Albuquerque, J. E.; Mattoso, L. H. C.; Faria, R. M.; Masters, J. G.; MacDiarmid, A. G. Study of the Interconversion of Polyaniline Oxidation States by Optical Absorption Spectroscopy. *Synth. Met*. **2004**, 146, 1-10.
19. Snape, J. B.; Nakajima, M. Processing of Agricultural Fats and Oils Using Membrane Technology. *J. Food Eng*. **1996**, 30, 1-41.
20. Shi, G. M.; Davood Abadi Farahani, M. H.; Liu, J. Y.; Chung, T.-S. Separation of Vegetable Oil Compounds and Solvent Recovery Using Commercial Organic Solvent Nanofiltration Membranes. *J. Membr. Sci*. **2019**, 588, 117202.
21. Badan Ribeiro, A. P.; Bei, N.; Guaraldo Gonçalves, L. A.; Cunha Petrus, J. C.; Viotto, L. A. The Optimisation of Soybean Oil Degumming on a Pilot Plant Scale Using a Ceramic Membrane. *J. Food Eng*. **2008**, 87, 514-521.
22. Pagliero, C.; Ochoa, N. A.; Martino, P.; Marchese, J. Separation of Sunflower Oil from Hexane by Use of Composite Polymeric Membranes. *J. Am. Oil Chem. Soc*. **2011**, 88, 1813-1819.
23. Köseoglu, S. S.; Lawhon, J. T.; Lusas, E. W. Membrane Processing of Crude Vegetable Oils: Pilot Plant Scale Remoyal of Solvent From Oil Miscellas. *J. Am. Oil Chem. Soc*. **1990**, 67, 315-322.
24. Chi-Sheng Wu, J.; Lee, E.-H. Ultrafiltration of Soybean Oil/ hexane Extract by Porous Ceramic Membranes. *J. Membr. Sci*. **1999**, 154, 251-259.
25. Rama, L. P.; Cheryan, M.; Rajagopalan, N. Solvent Recovery and Partial Deacidification of Vegetable Oils by Membrane Technology. *Lipid/Fett*, **1996**, 98, 10-14.
26. Kuk, M. S.; Hron, R. J.; Abraham, G. Reverse Osmosis Membrane Characteristics for Partitioning Triglyceride-solvent Mixtures. *J. Am. Oil Chem. Soc*. **1989**, 66, 1374-1380.
27. Jimenez-Solomon, M. F.; Gorgojo, P.; Munoz-Ibanez, M.; Livingston, A. G. Beneath the Surface: Influence of Supports on Thin Film Composite Membranes by Interfacial Polymerization for Organic Solvent Nanofiltration. *J. Membr. Sci*. **2013**, 448, 102-113.
28. Chen, D.; Miao, Y.-E.; Liu, T. Electrically Conductive Polyaniline/Polyimide Nanofiber Membranes Prepared via a Combination of Electrospinning and Subsequent *In situ* Polymerization Growth. *ACS Appl. Mater. Interfaces* **2013**, 5, 1206-1212.
29. Soroko, I.; Sairam, M.; Livingston, A. G. The Effect of Membrane Formation Parameters on Performance of Polyimide Membranes for Organic Solvent Nanofiltration (OSN). Part C. Effect of Polyimide Characteristics. *J. Membr. Sci*. **2011**, 381, 172-182.
30. Jimenez Solomon, M. F.; Bhole, Y.; Livingston, A. G. High flux Membranes for Organic Solvent Nanofiltration (OSN)—Interfacial Polymerization with Solvent Activation. *J. Membr. Sci*. **2012**, 423, 371-382.
31. Fontananova, E.; Di Profio, G.; Artusa, F.; Drioli, E. Polymeric Homogeneous Composite Membranes for Separations in Organic Solvents. *J. Appl. Polym. Sci.* **2012**, 129, 1653-1659.
32. See Toh, Y. H.; Loh, X. X.; Li, K.; Bismarck, A.; Livingston, A. G. In Search of a Standard Method for the Characterisation of Organic Solvent Nanofiltration Membranes. *J. Appl. Polym. Sci*., **2007**, 291, 120-125.
33. See Toh, Y. H.; Lim, F. W.; Livingston, A. G. Polymeric Membranes for Nanofiltration in Polar Aprotic Solvents. *J. Membr. Sci*. **2007**, 301, 3-10.
34. Abdellah, M. H. A. The use of Membrane Technology for Vegetable Oil processing with Green Solvents. Ph. D. Thesis, The University of Melbourne, Australia, 2019.
35. Wahab, M. Y.; Muchtar, S.; Arahman, N.; Mulyati, S.; Riza, M. The Effects of Solvent Type on The Performance of Flat Sheet Polyethersulfone/Brij58 Membranes. *IOP Conf. Ser.: Mater. Sci. Eng*. **2019**, 536, 012119.
36. Behnke, S.; Ulbricht, M. Two New Preparations for Organophilic Nanofiltration Membranes Based on Photocrosslinked Polyimide. *Procedia Eng*. **2012**, 44, 244-246.
37. Kazimierska, E.; Muchindu, M.; Morrin, A.; Iwuoha, E.; Smyth, M. R.; Killard, A. J. The Fabrication of Structurally Multiordered Polyaniline Films and Their Application in Electrochemical Sensing and Biosensing. *Electroanalysis* **2009**, 21, 595-603.
38. Yusoff, I. I.; Rohani, R.; Khairul Zaman, N.; Junaidi, M. U. M.; Mohammad, A. W.; Zainal, Z. Durable Pressure Filtration Membranes Based on Polyaniline-polyimide P84 Blends. *Polym. Eng. Sci*. **2018**, 59, E82-E92.
39. Liu, Y.; Wang R.; Chunga, T.-S. Chemical Cross-linking Modification of Polyimide Membranes for Gas Separation. *J. Membr. Sci*. **2001**, 189, 231-239.

40. Ahmad, M.; Qaiser, A. A.; Huda, N. U.; Saeed, A. Heterogeneous Ion Exchange Membranes Based on Thermoplastic Polyurethane (TPU): Effect of PSS/DVB Resin on Morphology and Electrodialysis. *RSC Adv.* **2020**, 10, 3029-3039.
41. Kim, E.; Choi, M. Effects of Electrodeposition Methods on Electrochemical and Morphological Properties of Polyaniline. *Polym. Korea* **2016**, 40, 728.
42. Man, J.; Obrtlík, K.; Blochwitz, C.; Polák, J. Atomic Force Microscopy of Surface Relief in Individual Grains of Fatigued 316l Austenitic Stainless Steel. *Acta Mater*. **2002**, 50, 3767-3780.
43. Shehzad, M. A.; Qaiser, A. A.; Javaid, A.; Saeed, F. *In Situ* Solution-phase Polymerization and Chemical Vapor Deposition of Polyanilne on Microporous Cellulose Ester Membranes: AFM and Electrical Conductivity Studies. *Synth. Met*. **2015**, 200, 164-171.
44. Qaiser, A. A.; Hyland, M. M.; Patterson, D. A. Surface and Charge Transport Characterization of Polyaniline−Cellulose Acetate Composite Membranes. *J. Phys. Chem. B* **2011**, 115, 1652-1661.
45. Qiao, Z.; Wang, Z.; Zhang, C.; Yuan, S.; Zhu, Y.; Wang, J.; Wang, S. PVAm-PIP/PS Composite Membrane with High Performance for CO_2/N_2 Separation. *AIChE J*. **2012**, 59, 215-228.
46. Ma, W.; Li, T.; Jiang, C.; Zhang, P.; Deng, L.; Xu, R.; Zhang, Q.; Zhong, J.; Matsuyama, H. Effect of Chain Structure on the Solvent Resistance in Aprotic Solvents and Pervaporation Performance of PMDA and BTDA Based Polyimide Membranes. *J. Membr. Sci*. **2019**, 584, 216-226.
47. Mostafaei, A.; Zolriasatein, A. Synthesis and Characterization of Conducting Polyaniline Nanocomposites Containing ZnO Nanorods. *Prog. Nat. Sci. Mater. Int*. **2012**, 22, 273-280.
48. Tres, M. V.; Racoski, J. C.; Novello, Z.; de Melo, J. R. M.; Ferraz, H. C.; Di Luccio, M.; Oliveira, J. V. Separation of Soybean Oil/*n*-hexane Miscellas Using Polymeric Membranes. *J. Food Sci. Eng*. **2012**, 2, 616-624.
49. Mubofu, E. B. Castor Oil as A Potential Renewable Resource for the Production of Functional Materials. *Sustain. Chem. Process*. **2016**, 4, 11.
50. Mänttäri, M.; Nyström, M. Negative Retention of Organic Compounds in Nanofiltration. *Desalination* **2006**, 199, 41-42.
51. Yaroshchuk, A. E.; Negative Rejection of Ions in Pressure-driven Membrane Processes. *Adv. Colloid Interface Sci*. **2008**, 139, 150-173.
52. Van der Bruggen, B.; Schaep, J.; Wilms, D.; Vandecasteele, C. Influence of Molecular Size, Polarity and Charge on the Retention of Organic Molecules by Nanofiltration. *J. Membr. Sci*. **1999**, 156, 29-41.
53. Zhang, L.; Zhang, L.; Wan, M.; Wei, Y. Polyaniline Micro/Nanofibers Doped with Saturation Fatty Acids. *Synth. Met*. **2006**, 156, 454-458.
54. Nagarale, R.; Gohil, G.; Shahi, V. K.; Trivedi, G.; Rangarajan, R. Preparation and Electrochemical Characterization of Cation- and Anion-exchange/Polyaniline Composite Membranes. *J. Colloid Interface Sci*. **2004**, 277, 162-171.
55. Rustan, A. C.; Drevon, C. A. Fatty Acids: Structures and Properties, In *Encyclopedia of Life Sciences*, Wiley: Chicheste, UK, 2005; pp 1-7.
56. Ahmad, M. U. Ed., Fatty Acids: Chemistry, synthesis, and applications, Elsevier: Kidlington, UK, 2017.